Fast Kinetics of Taxol Binding to Microtubules

EFFECTS OF SOLUTION VARIABLES AND MICROTUBULE-ASSOCIATED PROTEINS*

José Fernando Díaz‡, Isabel Barasoain, and José Manuel Andreu
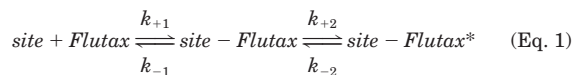
From the Centro de Investigaciones Biológicas, Consejo Superior de Investigaciones Científicas, C/Velázquez, 144. 28006 Madrid, Spain

The kinetics of Taxol association to and dissociation from stabilized microtubules has been measured by competition with the reference fluorescent derivative Flutax-1 (Díaz, J. F., Strobe, R., Engelborghs, Y., Souto, A. A., and Andreu, J. M. (2000) *J. Biol. Chem.* 275, 26265–26276). The association rate constant at 37 °C is $k_+ = (3.6 \pm 0.1) \times 10^6 \, \text{M}^{-1} \, \text{s}^{-1}$. The reaction profile is similar to that of the first step of Flutax-1 binding, which probably corresponds to the binding of the Taxol moiety. The rate constant of the initial binding of Flutax-1 is inversely proportional to the viscosity of the solution, which is compatible with a diffusion-controlled reaction. Microtubule-associated proteins bound to the microtubule outer surface slow down the binding of Flutax-1 and Flutax-2 10-fold. The binding site is fully accessible to Flutax-2 in native cytoskeletons of PtK2 cells; the observed kinetic rates of Flutax-2 microtubule staining and de-staining are similar to the reaction rates with microtubule associated proteins-containing microtubules. The kinetic data prove that taxoids bind directly from the bulk solution to an exposed microtubule site. Several hypotheses have been analyzed to potentially reconcile these data with the location of a Taxol-binding site at the model microtubule lumen, including dynamic opening of the microtubule wall and transport from an initial Taxol-binding site at the microtubule pores.

Taxol,[1] a complex diterpene found in the bark of the Pacific yew (1), is a recent addendum to the pharmacopeia of cancer treatment. Taxol is extensively used in the therapy of ovarian cancer, metastatic breast cancer, head and neck cancer, and lung cancer (2). At the time of the discovery of its action on microtubules (3), Taxol had a unique characteristic against other microtubule-binding drugs (4). Classical antimitotics (colchicine and vinblastine) bind to tubulin and prevent the

formation of microtubules (5–8). Taxol activates tubulin by binding to the microtubules, stabilizing the assembled form, and blocking the microtubule dynamics necessary for cell function (9–11). Taxol is able to drive the assembly of the otherwise inactive GDP-bound tubulin into microtubules (12). Recently, promising new microtubule-stabilizing anti-cancer drugs have been discovered, including cytotoxic products from myxobacterias (epothilones (13)), sea sponges (discodermolide (14) and laulimalide (15)), and a soft marine coral (eleutherobin (16)). Despite the different chemical structures of these compounds, they share a common pharmacophore with Taxol (17–20) and bind to the Taxol-binding site with different affinities,[2] except laulimalide (15), which binds at a different site in microtubules (21). The conformation of microtubule-bound Taxol has thoroughly been investigated (20, 22, 23).

The binding site of Taxol has been mapped in the β-tubulin subunit using photolabeling (24–26). The labeled amino acid residues are in agreement with the 3.5-Å resolution electron crystallographic structure of tubulin in Taxol-stabilized zinc-induced two-dimensional crystals (23, 27). Tubulin zinc sheets, whose assembly is not GTP-dependent (28), consist of protofilaments similar to those that form the microtubules although in an antiparallel array. The docking of these protofilaments into electron microscopy density maps of Taxol-containing 14 and 15 protofilament microtubules (29, 30) results in an atomic model of microtubules in which the binding site of Taxol is located on the microtubule inner surface (30, 31). Such luminal location will in principle make the binding site difficult to access for Taxol site ligands in assembled microtubules. However, it had been shown previously that Taxol modifies the flexibility of microtubules in a few seconds (32) and that the reversible binding of Taxol and its side chain analog docetaxel to an accessible site of microtubules changes the number of their protofilaments within a time range of 1 min (33). The binding site of Taxol is easily accessible for two fluorescent derivatives of Taxol, Flutax-1 and Flutax-2 (34, 35). These probes easily bind to and dissociate from native cytoplasmic and spindle microtubules and centrosomes and are able to induce cell death (34, 36). The binding of these ligands takes place in a two-step mechanism (35) as shown in Equation 1,

$$site + Flutax \underset{k_{-1}}{\overset{k_{+1}}{\rightleftharpoons}} site - Flutax \underset{k_{-2}}{\overset{k_{+2}}{\rightleftharpoons}} site - Flutax^* \quad \text{(Eq. 1)}$$

The first step comprises the fast binding of the ligand with micromolar affinity. This reaction does not affect the mobility of the fluorescent group (either fluorescein or difluorofluorescein), and because it is blocked by docetaxel it seems to be contributed to by the binding of the Taxol moiety itself. The

[1] The abbreviations used are: Taxol® (Bristol-Myers Squibb Co.) (paclitaxel), 4,10-diacetoxy-2*a*-(benzoyloxy)-5*b*,20-epoxy-1,7*b*-dihydroxy-9-oxotax-11-en-13*a*-yl(2*R*,3*S*)-3-[(phenylcarbonyl)amino]-2-hydroxy-3-phenylpropionate; docetaxel (Taxotere®), 4-acetoxy-2*a*-(benzoyloxy)-5*b*,20-epoxy-1,7*b*,10*b*-trihydroxy-9-oxotax-11-en-13*a*-yl(2*R*,3*S*)-3-[(*tert*-butoxycarbonyl)amino]-2-hydroxy-3-phenylpropionate; Flutax-1, (7-*O*-[*N*-(4′-fluoresceincarbonyl)-L-alanyl]Taxol; Flutax-2, (7-*O*-[*N*-(2,7-difluoro-4′-fluoresceincarbonyl)-L-alanyl]Taxol; MAPs, microtubule-associated proteins; Mes, 4-morpholineethanesulfonic acid; Pipes, 1,4-piperazinediethanesulfonic acid; GMPCPP, guanosine 5′-(α,β-methylene)triphosphate.

[2] J. F. Díaz, unpublished data.

kinetic binding constants k_{+1} are of the order of 10^6 M^{-1} s^{-1} at 37 °C (35) indicating binding to an exposed binding site, in contrast with the current microtubule model. Subsequent to the bimolecular step, there is a monomolecular reaction that involves a rearrangement in the system resulting in the immobilization of the fluorescent group. This step probably implies a weak binding of the fluorescein moiety to the microtubules (35).

The purpose of this study was to definitely establish the accessibility of the binding site of Taxol in microtubules. Therefore, the kinetics of Taxol association and dissociation have been measured in order to discard any possible enhancement of the association rates by the fluorescent side chain of the analogs. Thus, these fluorescent derivatives of Taxol were used to learn about the mechanisms that allow such accessibility by investigating the effects of the solution variables and possible perturbants on the binding kinetics, such as the presence or absence of MAPS and the C-terminal acidic segment of tubulin. The binding rates of fluorescent taxoids to the Taxol site in native microtubule cytoskeletons have been measured as well. Finally, several hypotheses have been analyzed to potentially reconcile the location of the binding site of Taxol in the lumen of model microtubules with fast binding kinetics.

EXPERIMENTAL PROCEDURES

Tubulin and Taxoids—Purified calf brain tubulin and chemicals were as described (12). For glycerol-induced assembly, tubulin was directly equilibrated in buffer: 10 mM phosphate, 1 mM EGTA, 0.1 mM GTP, 3.4 M glycerol, pH 6.8. All tubulin samples were clarified by centrifugation at 50,000 rpm, 4 °C, for 10 min using TL100.2 or TL100.4 rotors in Beckman Optima TLX centrifuges. After centrifugation, 6 mM MgCl$_2$ and up to 1 mM GTP were added to the solution, giving a final pH 6.5. Microtubular protein, containing tubulin and MAPs, was prepared as described (37) in 100 mM Mes, 1 mM EGTA, 1 mM MgSO$_4$, 2 mM 2-mercaptoethanol, 1 mM GTP, pH 6.5. MAPs were prepared from microtubular protein as described (38). hTau40, the longest isoform of microtubule-associated protein Tau (39), was a gift from Dr. Vincent Peyrot and François Devred (University of Marseille, France). It was dissolved in 10 mM phosphate, pH 6.5, buffer, and its concentration was determined spectrophotometrically in 6 M guanidinium chloride (employing a practical extinction coefficient of 6500 M^{-1} cm^{-1} at 280 nm, computed using the ProtParam tool at www.expasy.ch). The activity of both MAPS and Tau was confirmed by means of a cosedimentation assay with cross-linked microtubules. Docetaxel (Taxotere®) was kindly provided by Rhône-Poulenc Rorer (92165 Antony, France). Flutax-1 (7-*O*-[*N*–(4′-fluoresceincarbonyl)-L-alanyl]-Taxol) and Flutax-2 (7-*O*-[*N*–(4′-2,7-difluoro-fluoresceincarbonyl)-L-alanyl]-Taxol) were synthesized as described (40).

The diffusion coefficients of the taxoids were measured at 20 °C in 10 mM phosphate, pH 6.5, buffer using a synthetic boundary cell in an Optima XL-A (Beckman Instruments) analytical ultracentrifuge as described (41) at a speed of 15,000 rpm and wavelength of 230 (Taxol and docetaxel) or 495 nm (Flutax-1 and Flutax-2). The data were analyzed using the program VELGAMMA (42). The diffusion coefficients in GAB (glycerol assembly buffer, 3.4 M glycerol, 10 mM sodium phosphate, 1 mM EGTA, 6 mM MgCl$_2$, 0.1 mM GTP, pH 6.5) at 37 °C were calculated from the values in phosphate buffer using the viscosity of a 30% solution of glycerol in water at 37 °C (1.55 centipoise (43)).

Preparation of Stabilized Microtubules—Solutions of 50 μM tubulin in GAB were assembled at 37 °C for 30 min, and 20 mM glutaraldehyde was added to the solution, which was kept at 37 °C for another 10 min. The remains of the cross-linking agent were quenched by adding 60 mM NaBH$_4$ (Fluka), and the solution was dialyzed overnight using Slide-A-Lyzer 10K dialysis cassettes (Pierce) against the desired buffer and drop-frozen in liquid nitrogen (35, 44). After this treatment 90% of the tubulin was found to have incorporated into the microtubules, and 100% of the assembled tubulin dimers were found to bind taxoids immediately after dialysis (as measured by a sedimentation assay (35)). Each batch of cross-linked microtubules was found to be stable against dilution and low temperatures. The binding sites of Taxol in drop-frozen microtubules were found to be stable for at least several months, while they slowly decayed at 4 °C with a half-life of ~50 days (average of four batches).

The morphology of the cross-linked microtubules was checked with electron microscopy as described previously (45). Cross-linked microtu-

bules before freezing were normal and indistinguishable from non-stabilized microtubules, whereas unfrozen microtubules showed many openings along their structures.

When indicated, cross-linked microtubules in GAB 0.1 mM GTP were digested with 0.7% w/w subtilisin Carlsberg (Sigma) for 30 min at 37 °C. The reaction was stopped with 2 mM phenylmethylsulfonyl fluoride (Calbiochem), and the cleavage of the C-terminal fragment of both tubulin subunits was checked by SDS-PAGE of peptides (46).

Kinetics of Taxoids Binding to and Dissociation from Microtubules—The kinetics of binding and dissociation of Flutax-1 and Flutax-2 were measured by the change of fluorescence intensity using an SS-51 stopped flow device (High-Tech Scientific, UK) equipped with a fluorescence detection system, using an excitation wavelength of 492 and a 530-nm cut-off filter in the emission pathway. The fitting of the kinetic curves was done with a non-linear least squares fitting program based on the Marquardt algorithm (47) where pseudo-first order conditions were used; otherwise the FITSIM package (48) was employed.

Because the binding of Taxol to microtubules does not produce any optical signal, its binding kinetics was measured by its effect on the observable Flutax-1 binding to microtubules. The binding of Flutax-1 to its microtubule site in the presence of different concentrations of Taxol was measured as described above. The kinetic curves were fitted using the rate constants of binding and dissociation of Flutax-1 that had been determined independently (see Ref. 35 and this work).

The kinetics of dissociation of Taxol from its site in the microtubules was measured by adding 10 μM Flutax-1 to a solution containing 1 μM Taxol and 1 μM binding sites. The dissociation of Taxol can be assessed by the small (less than 5%) change in fluorescence intensity of the solution because of the binding of Flutax-1 to the sites left empty by Taxol. The low signal to noise ratio required averaging a minimum of 10 experimental curves per measurement. These experiments were measured with a photon counting instrument Fluorolog 3-221 (Jobin Yvon-Spex, Longiumeau, France) with excitation wavelength 495 nm (0.1-nm bandpass in order to prevent photolysis) and emission wavelength 525 nm (5-nm bandpass).

The equilibrium binding constants of Flutax-1, Flutax-2, and Taxol to microtubules were obtained from anisotropy titration measurements made with a PolarStar microplate reader (BMG Labtechnologies, Offenburg, Germany) at different temperatures, as described (44).

Cytoskeletons and Fluorescence Microscopy—PtK2 potoroo epithelial-like kidney cells were cultured as described previously (49). Unfixed coverslip-attached PtK2 cytoskeletons were obtained by washing cells eight times with PEMP (PEM buffer containing 4% polyethylene glycol 8000, pH 6.8), and then the cells were permeabilized with 0.5% (v/v) Triton X-100 in PEM (100 mM Pipes, 1 mM EGTA, 1 mM MgCl$_2$, pH 6.8) for 90 s at room temperature and finally washed eight times in PEMP microtubule stabilizing buffer (34) to avoid disassembly. The cytoskeletons were dipped into 0.2 or 1 μM Flutax-2 for different times. They were rapidly washed 12 times with 2 ml of PEMP changing the washing well after six washes, mounted with 20 μl of PEMP, and their images were recorded with a Zeiss Axioplan epifluorescence microscope using a 100× Plan-Apochromat objective and a Hamamatsu 9742-95 cooled CCD camera (36). Controls were performed, in which the incubation with Flutax-2 was made in the presence of 50 μM docetaxel (which was preferred to Taxol due to its higher solubility). The displacement of Flutax-2 was observed in cytoskeletons incubated for 2 min with 1 μM Flutax-2, washed eight times with PEMP in two different wells, incubated with 13.3 μM docetaxel for different times, and then washed again eight times with PEMP in two different wells to remove the displaced Flutax-2, and the images were recorded as above.

The fluorescence intensities of a minimum of 10 different fields per time point were integrated using Scion Image (Scion Corp.) and averaged. In order to measure the fluorescence intensity per unit of length of microtubules, 3 × 10-pixel (0.08×0.24 μM) rectangles where defined over single interphasic microtubules in the images. The intensity of the rectangles was found to be homogeneous within each microtubule and among microtubules at each reaction time (the S.D. was $8 \pm 2\%$ of the mean value). The values of the controls performed with 50 μM docetaxel were subtracted from the data.

The maximal amount of tubulin contained in the cytoskeletons can be roughly estimated from the number of cells attached to the coverslip (~200,000) and the volume of each cell (~10^{-12} liters). Assuming that the concentration of cytoskeletal tubulin inside the cells is in the order of 50 μM (5 mg/ml), the maximal amount of tubulin per coverslip is 10^{-11} mol, which is 200 and 40 times lower than the amount of Flutax-2 (0.2 or 1 μM) in the 2-ml well. The fact that the concentration of Flutax-2 remains constant during the experiment (pseudo-first order conditions)

was confirmed by spectrophotometric measurements of Flutax-2 before and after staining of the cytoskeletons, with no change detected.

RESULTS

Kinetics of Taxol Binding to and Dissociation from Stabilized Microtubules—In order to discard the possibility that the fluorescein moiety of the fluorescent taxoids could contribute to the fast initial binding steps of these ligands to their site in the microtubules, the kinetic constants of Taxol association and dissociation were measured using a competition method. This method precludes analysis of the exact mechanism of association of Taxol, which is assumed to occur in a single step, thought to be equivalent to the first step of binding of Flutax-1 (Introduction). The microtubules used for these experiments had been stabilized by gentle cross-linking (see "Experimental Procedures"), a procedure that has been shown not to modify the kinetics of binding of fluorescent taxoids (35). Because the microtubules were frozen in liquid nitrogen and unfrozen prior to use, adequate controls were performed in order to check that the kinetics of binding was not modified by freezing, as was the case. The binding time course of 500 nM Flutax-1 to 500 nM sites was monitored in the presence of increasing concentrations of Taxol, using stopped flow techniques. If the association of Taxol were much slower than that of Flutax-1, no effect should be observed when increasing the concentration of Taxol. On the other hand, if the association of Taxol is faster than or comparable with that of Flutax-1, both Taxol and Flutax-1 will bind simultaneously, and only part of the sites will fill with Flutax-1; in this way an appreciable effect in the amplitude of the observed kinetics should be noticed. This is the case, as can be seen in Fig. 1*A*. A complete set of curves at each temperature were simultaneously fitted (using the rate constants of association and dissociation of Flutax-1 (35)), rendering the kinetic constants of Taxol binding to its site in the microtubules (Table I). The binding rate constant value determined at 37 °C is five times higher than that of the fast step of Flutax-1 association (Taxol, 3.6×10^6 M^{-1} s^{-1}; Flutax-1, 6.1×10^5 to 7.4×10^5 M^{-1} s^{-1} (35)) and less dependent on temperature, which indicates lower activation energy (Fig. 2*A*).

Additionally, in order to correlate the kinetic constants with the diffusion of the ligands, the diffusion coefficients of Taxol, Flutax-1, and Flutax-2 were measured in 10 mM phosphate buffer pH 7.0. The values determined in this aqueous buffer at 20 °C, $D_{20}H_2O$, are as follows: $3.1 \pm 0.3 \times 10^{-10}$ m^2 s^{-1} for Taxol, $2.8 \pm 0.2 \times 10^{-10}$ m^2 s^{-1} for Flutax-1, and $2.7 \pm 0.1 \times 10^{-10}$ m^2 s^{-1} for Flutax-2. After correction for the viscosity of GAB and temperature, the diffusion constants under the experimental conditions, D_{37},GAB, were $2.2 \pm 0.2 \times 10^{-10}$ m^2 s^{-1}, $1.9 \pm 0.2 \times 10^{-10}$ m^2 s^{-1}, and $1.8 \pm 0.2 \times 10^{-10}$ m^2 s^{-1}, respectively. The value of Flutax-2 is very close to the rough spherical approximation used in our previous work, 1.6×10^{-10} m^2 s^{-1} (35). The diffusion coefficient values of the fluorescent ligands indicate, following the Stokes-Einstein equation, an effective radius of 8 Å.

The kinetic constants of dissociation of Taxol were determined by displacing the Taxol bound to its site in the microtubules with a 10-fold excess of Flutax-1 (Fig. 1*B*). The values obtained for k_{-1} of Taxol (0.091 s^{-1} at 37 °C) (Table I) and its activation energy (Fig. 2*A*) are in between those of k_{-1} and k_{-2} of Flutax-1, so it is not possible to assign directly the dissociation step to either of the two dissociation steps of the fluorescent taxoid.

The ratio of k_+ and k_- renders equilibrium binding constant values of Taxol binding in the order of 10^7 M^{-1} s^{-1} which is compatible with equilibrium measurements of competition with Flutax-2 (Table II). There is a factor from 3 to 4 between both sets of values, coming from a similar factor observed
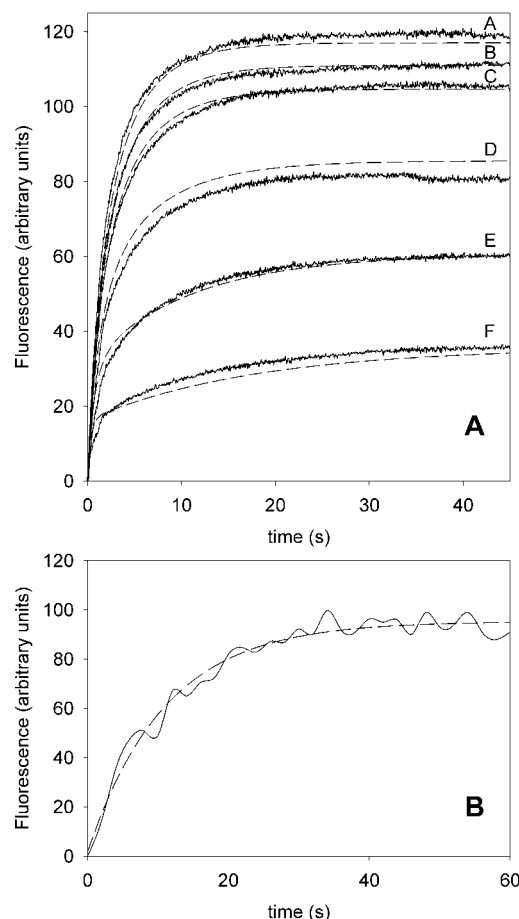

FIG. 1. *A*, kinetics of association of Taxol to microtubules at 37 °C. In the stopped flow device a solution of cross-linked microtubules containing 1 μM sites was mixed 1:1 with a 1 μM solution of Flutax-1, containing different concentrations of Taxol 0 μM (*curve A*), 0.05 μM (*curve B*), 0.1 μM (*curve C*), 0.25 μM (*curve D*), 0.5 μM (*curve E*), and 1 μM (*curve F*). The *dashed lines* are the result of the simultaneous fitting of all curves to a kinetic model of a single step association of Taxol. *B*, kinetics of dissociation of Taxol from microtubules at 37 °C. At time 0 s, 10 μM Flutax-1 was added to 1 μM binding sites in cross-linked microtubules that contained 1 μM Taxol. The reaction was followed by the change in fluorescence intensity (average of 9 curves). The data were smoothed in 1-s intervals, and fitted to a single exponential (*dashed line*).

between the equilibrium constants of the fluorescent taxoids used as reference values calculated from their kinetic parameters and those measured directly (Tables II and III in Ref. 35).

Effect of Solution Variables in the Kinetics of Binding of Flutax-1 to Stabilized Microtubules—Once the fast binding of Taxol to stabilized microtubules had been characterized, and shown to be clearly related to the first step of the association of Flutax-1, and the accessibility of the taxoid-binding site in the microtubules proved to be independent from the existence of the fluorescent moiety of Flutax-1 and Flutax-2, these fluorescent taxoids could be used as *bona fide* probes of the kinetics of binding and therefore were used for the rest of the study. Because Flutax-1 has a larger fluorescence intensity change upon binding, it was preferred for the stopped flow studies.

The first step of Flutax-1 and Flutax-2 binding to microtubules has been proposed to be a diffusion-collision reaction (35). To confirm this, the dependence of the association rate constant on viscosity was studied using GAB buffers with different concentrations of glycerol (0–60% instead of the usual 30%). If one of the reactants is as large as a microtubule and diffusion controls the reaction, the association rate constant will depend on the diffusion coefficient of the ligand (see Equation 3 in Ref.

TABLE I

Kinetics constants of Taxol association to (k_{+1}) and dissociation from (k_{-1}) cross-linked microtubules

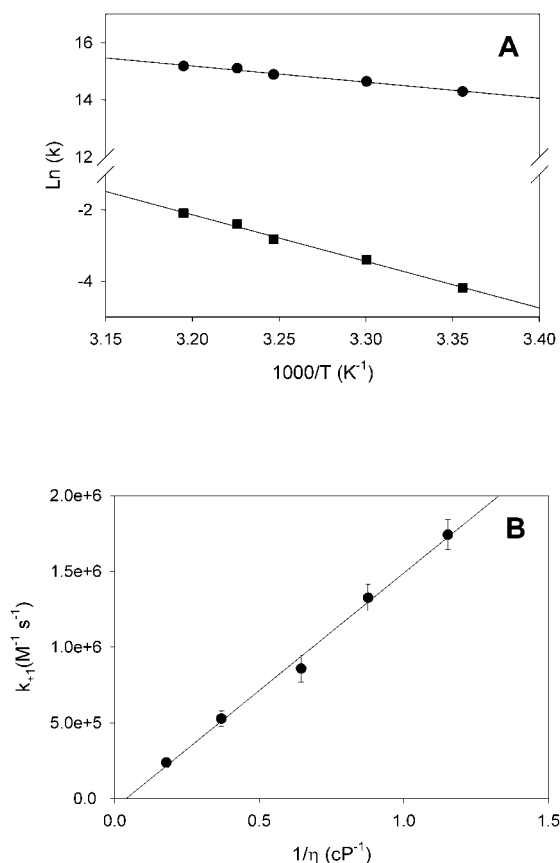|	25 °C	30 °C	35 °C	37 °C	40 °C
k_{+1} ($\times 10^6$ M^{-1} s^{-1})	1.61 ± 0.10	2.29 ± 0.06	2.93 ± 0.09	3.63 ± 0.08	3.91 ± 0.05
k_{-1} ($\times 10^{-2}$ s^{-1})	1.52 ± 0.10	3.34 ± 0.18	5.92 ± 0.41	9.10 ± 0.62	12.37 ± 0.88

FIG. 2. *A*, Arrhenius plots of the association and dissociation of the Taxol-microtubules complex. *Solid circles,* association rate constants of Taxol binding. *Solid squares,* rate constants of Taxol dissociation. *B*, dependence on the buffer viscosity of k_{+1} of Flutax-1 binding. All reactions were performed in 10 mM phosphate, 1 mM EGTA, 6 mM MgCl$_2$, 0.1 mM GTP, pH 6.5, plus different concentrations of glycerol from 0 to 60% v/v.

35), which is inversely proportional to the viscosity of the medium, as shown by the Stokes-Einstein equation. As can be seen in Fig. 2*B*, k_{+1} linearly depends on the reciprocal of the viscosity of the media as expected from a diffusion-collision reaction.

The association of Flutax-1 to cross-linked microtubules was also studied under different conditions *e.g.* buffer composition, pH, ionic strength, and Mg^{2+} concentration, in order to learn from the system by observing the changes induced by these solution variables. The results (Table III) can be summarized as follows: (*a*) lowering the pH accelerates the binding reaction; (*b*) a moderate ionic strength doubles the reaction rate; and (*c*) Mg^{2+} seems to be a requirement for Flutax-1 binding.

Effect of Modifying the Outer Surface of Microtubules; Kinetics of Binding of Flutax-1 and Flutax-2 to MAP-containing Microtubules—To know if the surface-bound MAPs affect the binding of taxoids to the microtubules, kinetic studies were performed using microtubules stabilized by MAPs (instead of cross-linking). Fig. 3*A* shows the time course of binding of Flutax-1 to microtubules assembled from microtubular protein in AB buffer (microtubular protein assembly buffer, 100 mM Mes, 1 mM EGTA, 1 mM MgSO$_4$, 2 mM 2-mercaptoethanol, 0.1

mM GTP, pH 6.5) under pseudo-first order conditions. Two main differences from microtubules assembled from pure tubulin in GAB buffer can easily be observed (Fig. 3*B, dotted line*). First, the reaction is slower, with a half-life of 250 ms compared with 75 ms in similar reactant concentrations. Second, the curve cannot be described by single exponential decay but by the sum of two exponentials, indicating the presence of at least two different processes. Because, in order to assemble and stabilize microtubules by MAPs, AB buffer had to be employed, adequate control measurements[3] were performed that discarded the possibility that the observed effects could be due to the buffer change.

In order to confirm that the kinetic changes are truly due to the MAPs, and not to the differences in the tubulin purification methods, isolated MAPs were added in AB buffer to cross-linked microtubules, which remained stable in the presence of at least 15% w/w of MAPs. The same proportion of MAPs to microtubules was needed in order to turn the monophasic kinetics into biphasic kinetics, and 20% w/w was necessary to reconstitute the parameters of binding of Flutax-1 to microtubular protein in AB (Fig. 3*B*; 0% MAPS (*dotted line*), monophasic kinetics, k_+ 7.56 $\pm$ 0.49 $\times 10^5$ M^{-1} s^{-1}; 20% MAPS (*solid line*), biphasic kinetics, k_{+1} 2.18 $\pm$ 0.35 $\times 10^5$ M^{-1} s^{-1}, k_{+2} 2.43 s^{-1}, 35 °C; the amplitude of the slow phase was still smaller than in the case of binding to microtubules assembled from microtubular protein in AB buffer, even if 40% w/w MAPS were added). These results prove that the slowing down of the kinetics is a genuine effect of MAPs, and moreover support previous evidence that the cross-linking of purified tubulin microtubules does not modify their fluorescent taxoid binding properties, (35).

To know whether the kinetic changes might be due to shielding of the acidic C-terminal domains of tubulin by MAPS, the effect of the positively charged hTau40 on the kinetics were measured. The binding of recombinant hTau40 to microtubules negligibly modified the rate of binding of Flutax-1. Different proportions (from 0 to 20% mol/mol tubulin) of hTau40 were added to cross-linked microtubules in GAB, and the kinetics of association of Flutax-1 were measured at 37 °C (the k_{+1} values are as follows: 0%, 6.32 $\pm$ 1.12 $\times 10^5$ M^{-1} s^{-1}; 5%, 8.26 $\pm$ 1.22 $\times 10^5$ M^{-1} s^{-1}; 10%, 7.42 $\pm$ 1.54 $\times 10^5$ M^{-1} s^{-1}; 15%, 7.08 $\pm$ 1.01 $\times 10^5$ M^{-1} s^{-1}; 20%, 6.40 $\pm$ 0.97 $\times 10^5$ M^{-1} s^{-1}; the association curves were monophasic in all cases). The effect of 20% mol/mol hTau 40 in the rate constants of Flutax-1 was further studied at different temperatures, but no significant differences with the constants in the absence of hTau40 were found. The combination of changing the buffer to AB and the addition of 20% mol/mol of hTau40 did not reproduce the effect of MAPS (k_{+1} 37 °C, 23.58 $\pm$ 0.67 $\times 10^5$ M^{-1} s^{-1}, monophasic

---

[3] The kinetics of association of cross-linked microtubules made of purified tubulin Flutax-1 was measured in AB buffer in which microtubules are stable for a limited time. The rate value obtained for Flutax-1 at 37 °C (k_{+1} 20.28 $\pm$ 2.17 $\times 10^5$ M^{-1} s^{-1}) was three times faster than the rate measured in GAB. Nevertheless, the acceleration was due to the lower viscosity of the buffer, because addition of 3.4 M glycerol to AB buffer reduces the association constant to a value (k_{+1} 37 °C 9.42 $\pm$ 1.21 $\times 10^5$ M^{-1} s^{-1}) similar to those in GAB. The kinetics of association and dissociation of Flutax-1 to and from microtubular protein are not modified if 30% glycerol is added to AB (k_{+1} 37 °C 2.41 $\pm$ 0.25 $\times 10^5$ M^{-1} s^{-1}, k_{-2} 4.01 $\pm$ 0.23 $\times 10^{-2}$ s^{-1}), indicating that in this case the reaction is no longer diffusion-limited.

TABLE II

Experimental and calculated equilibrium constants and thermodynamic parameters of binding of Taxol to its site in cross-linked microtubules

	25 °C	30 °C	35 °C	37 °C	40 °C
$K (\times 10^7 \text{ M}^{-1})^a$	2.64 ± 0.17	1.83 ± 0.09	1.43 ± 0.17	1.07 ± 0.11	0.94 ± 0.23
$K (\times 10^7 \text{ M}^{-1})^b$	10.6 ± 1.4	6.9 ± 0.5	4.9 ± 0.6	4.0 ± 1.0	3.2 ± 0.5
$Ea_+ \text{ kJ mol}^{-1b}$				47 ± 4	
$Ea_- \text{ kJ mol}^{-1b}$				109 ± 5	
$\Delta H \text{ kJ mol}^{-1b}$				−62 ± 6	
$\Delta S \text{ J mol}^{-1} \text{ K}^{-1b}$				−53 ± 5	
$\Delta H \text{ kJ mol}^{-1a}$				−51 ± 4	
$\Delta S \text{ J mol}^{-1} \text{ K}^{-1a}$				−28 ± 13	

[a] Data from equilibrium competition measurements with Flutax-2 as reference.
[b] Data from kinetic competition measurements with Flutax-1 as reference.

TABLE III

Effect of solution variables in the association rate constant of Flutax-1 binding to microtubules in GAB

pH	$k_{+1} (\times 10^5 \text{ M}^{-1} \text{ s}^{-1})$	NaCl	$k_{+1} (\times 10^5 \text{ M}^{-1} \text{ s}^{-1})$	Mg^{2+}	$k_{+1} (10^5 \text{ M}^{-1} \text{ s}^{-1})$
		mm		*mm*	
6.25	13.25 ± 2.35	0	6.96 ± 0.53	0	No binding
6.5	6.96 ± 0.53	50	11.80 ± 1.59	3	5.89 ± 0.68
6.75	3.05 ± 0.38	500	11.54 ± 3.18	6	6.96 ± 0.53
7	1.58 ± 0.52				

kinetics). These results suggested that shielding of the acidic C-terminal domains of tubulin by the positively charged Tau is not enough to slow down the binding of Flutax-1, but another MAP component is required, for example, high molecular weight MAPs providing steric hindrance to the approaching ligand. In fact, reducing the negative surface charge of the microtubules by subtilisin proteolysis of the C-terminal segments of assembled microtubules (where the main differences between tubulin isotypes and most of the post-translational modifications are located (50, 51)) had no significant effect on the association rate (k_{+1} 37 °C non-digested microtubules, $6.34 \pm 1.00 \times 10^5$ M^{-1} s^{-1}; C-terminal cleaved microtubules $6.01 \pm 0.40 \times 10^5$ M^{-1} s^{-1}), suggesting as well no influence of the tubulin isotypes or post-translational modifications in the kinetics.

The kinetics of binding of Flutax-1 and Flutax-2 to microtubules with MAPS were quantitatively studied in AB buffer. Fig. 4 shows the dependence of the observed rate constants of binding of Flutax-1 at 37 °C on the concentration of sites. The fast constant depends linearly on the concentration of sites, although the slow phase saturates with the concentration of sites. This indicates a mechanism where binding is followed by a monomolecular reaction, similar to the one observed in the binding to microtubules assembled from pure tubulin in GAB (see Equation 1). Nevertheless, here the rate constant of the second step, the monophasic reaction, is still quite strongly dependent on the concentration of sites, which indicates that the equilibrium constant of the first step is lower than in the absence of MAPs, and so the reaction is not completely displaced toward the end product. The second step of the reaction is now observed, as it displaces the equilibrium toward the final state. Within such a model, if the difference between both constants is large enough (52), it is possible to determine the values of the individual kinetic constants from the values of the observed rate constants, as shown in Equations 2 and 3,

$$kf_{obs} = k_{+1} \cdot [\text{sites}] + k_{-1} \qquad \text{(Eq. 2)}$$

$$ks_{obs} = \frac{K_1 \cdot k_{+2} \cdot [\text{sites}]}{1 + K_1^* [\text{sites}]} + k_{-2} \qquad \text{(Eq. 3)}$$

where k_f(obs) and k_s(obs) are the observed rates of the fast and the slow phase, respectively.

From the data in Fig. 4 it is possible to determine the values of k_{+1} and k_{+2}. The value of k_{-1} can be determined (although
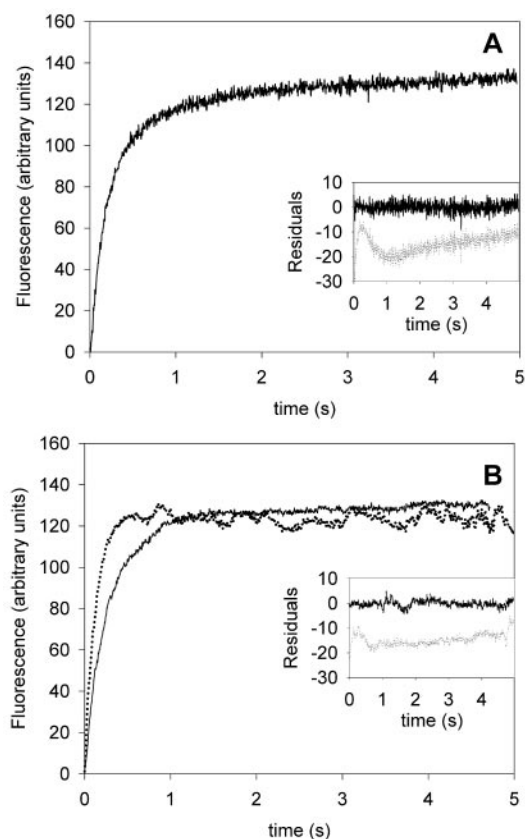

FIG. 3. *A*, kinetics of binding of Flutax-1 to MAP-containing microtubules at 35 °C. *Solid line*, in the stopped flow device a 1 μM solution of Flutax was mixed with 2.62 mg ml^{-1} microtubular protein in AB which contained 20 μM binding sites and ~20% MAPS (final concentrations 500 nM Flutax and 10 μM sites). The curve is fitted to a sum of two exponential decays. *Inset, dotted line*, residuals of the fitting to a single exponential; *solid line*, residuals of the fitting to a sum of two exponentials. The *dotted line* in the *inset* is shifted 15 units down in the *y* axis for clarity in the presentation. *B*, effect of added MAPS on the kinetics of binding of Flutax-1 to cross-linked microtubules. A 1 μM solution of Flutax-1 was mixed with 20 μM sites in cross-linked microtubules in AB in the presence (*solid line*) and absence (*dotted line*) of 0.4 mg ml^{-1} isolated MAPS (final concentrations 500 nM Flutax-1, 10 μM sites, 0.2 mg ml^{-1} MAPS). *Inset, dotted line*, residuals of the fitting to a single exponential; *solid line*, residuals of the fitting to a sum of two exponentials. The *dotted line* in the *inset* is shifted 15 units down in the *y* axis for clarity in the presentation.
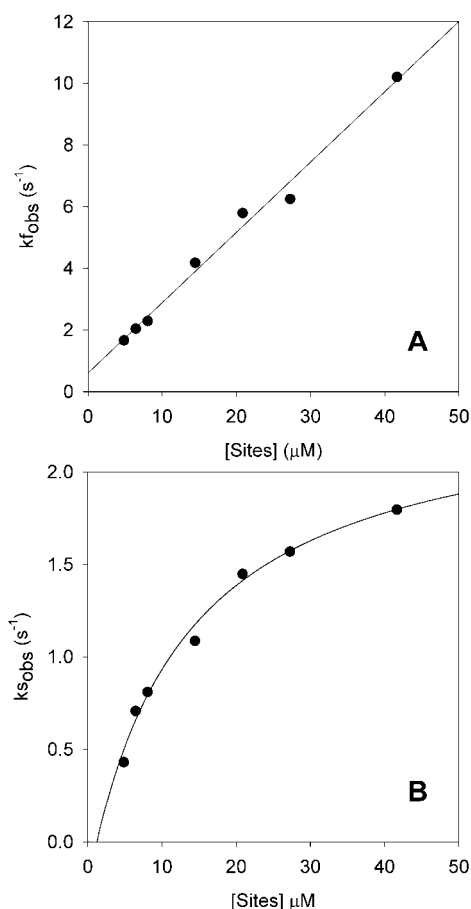
FIG. 4. **Dependence on the concentration of sites of the observed rate constants of fast and slow phases of the binding reaction of Flutax-1 to MAP-containing microtubules in AB at 37 °C (k_{fast} (*A*); k_{slow} (*B*)).** The *solid lines* are the best fittings to the experimental data.

FIG. 5. **Kinetics of dissociation of Flutax-1 from microtubules at 35 °C.** 200 μM docetaxel was mixed 1:1 with to 20 μM taxoid-binding sites in MAP-containing microtubules in AB which contained 15 μM Flutax-1 bound (final concentrations 100 μM docetaxel, 10 μM tubulin, 7.5 μM Flutax-1). Data are fitted to a single exponential.

with a large error margin) because its value is significant enough with respect to the product $k_{+1}\cdot$[sites]. Because k_{-2} is very small, the extrapolation to [sites] equal to 0 is too large to determine its value properly, which has to be determined by dissociation kinetics. The values of k_{-2} are around 2 orders of magnitude lower than those of k_{-1}; k_{-2} is the rate-limiting step of the dissociation reaction (as for the dissociation from microtubules assembled from pure tubulin in GAB). The rate constants of dissociation of Flutax-1 and Flutax-2 from their site in MAP-containing microtubules were measured in the same way as for the complex with microtubules assembled from pure tubulin (Table III in Ref. 35). The reaction kinetics was found to be monophasic (see Fig. 5), and the values obtained for the k_{off} rate were very similar to those obtained in absence of MAPS in GAB. The rate constants determined for Flutax-1 and Flutax-2 are summarized in Table IV. The comparison of the kinetic constants to those obtained for the binding of Flutax-1 and Flutax-2 to microtubules without MAPS (see Table II in Ref. 35) shows that only the rate of the first step (k_{+1}) is significantly reduced by a factor of 3–4 in the presence of MAPS, whereas the values of the other kinetic constants (k_{-1}, k_{+2}, and k_{-2}) are only marginally altered. The thermodynamic parameters of the binding of Flutax-1 and Flutax-2 to MAP-containing microtubules (Table V) do not show great differences from those obtained with purified tubulin microtubules, except for the reduction of the activation energy of the first step of the binding, the one affected. Curiously, the presence of MAPs reduces the activation energy of the binding of Flutax to values similar to those of Taxol itself. The parameters of the
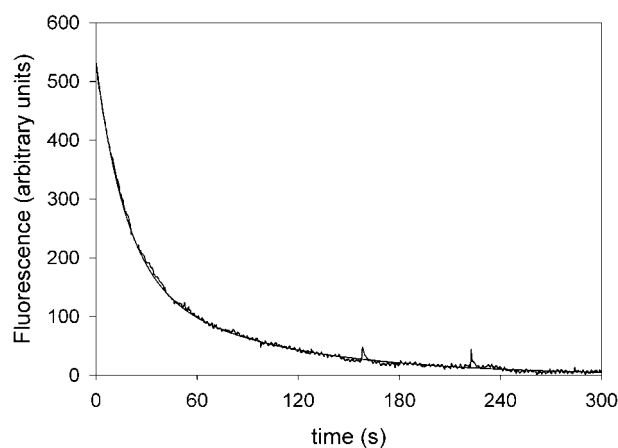
second step of the binding are very similar to those observed for the binding of Flutax-2 to the microtubules in GAB, which suggests that the immobilization of the fluorescein group is also very similar, and it is not affected by the presence of MAPS.

Kinetics of Binding of Fluorescent Taxoids to Microtubule Cytoskeletons—It might be argued that the kinetics of taxoid binding to *in vitro* assembled microtubules is not representative of cellular microtubules. In order to approach a more physiological situation and to know whether the accessibility of the binding site in native microtubules is similar to those assembled *in vitro*, the kinetics of the binding of fluorescent taxoid (Flutax-2 was chosen in this case due to its higher photostability) to native cytoskeletons from PtK2 cells at 25 °C has been semiquantitatively characterized by approaching pseudo-first order conditions, employing CCD-detected epifluorescence microscopy images (Fig. 6, *A–D*). The plot of the averaged fluorescence intensity *versus* incubation time (Fig. 6, *E* and *F*; 0.2 and 1 μM Flutax-2, respectively) shows an exponential staining of the cytoskeletons (the data do not permit us to distinguish between a single or double-exponential best fit). At 25 °C the half-lives of the binding process and 0.2 and 1 μM Flutax-2 are 80 and 12 s, respectively, which correspond to a value of k_+ of 6.1×10^4 M^{-1} s^{-1}. This value is compatible with the extrapolation to 25 °C of k_{+1} of Flutax-2 binding to *in vitro* assembled microtubules with MAPS which renders a rate constant of 1.3×10^5 M^{-1} s^{-1}. Docetaxel displaces Flutax-2 from its site in the microtubules with k_{obs} 0.75×10^{-2} s^{-1} (half-life in the range of 90 s (Fig. 7)). The dissociation rate constant of Flutax-2 from its site in microtubules assembled *in vitro* (Table IV) is k_{-2} $1.04 \times 10^{(2}$ s^{-1} (half-life of 66 s) which is close to the rate of the cytoskeleton destaining process.

In order to check if the staining and destaining was spatially homogeneous within a single microtubule (*i.e.* the complete microtubule stains and destains at the same time), the fluorescence intensity per unit of length of individual microtubules was measured. No differences were observed among different fragments of microtubules within the same image. It can be concluded from the data available that the kinetics of Flutax-2 binding to native microtubules from PtK2 cultured cells was not significantly different from the kinetics of binding to *in vitro* assembled MAP-containing microtubules.

DISCUSSION

Kinetics and Thermodynamics of Binding of Taxol and Fluorescent Taxoids to Microtubules—Because the exact kinetic
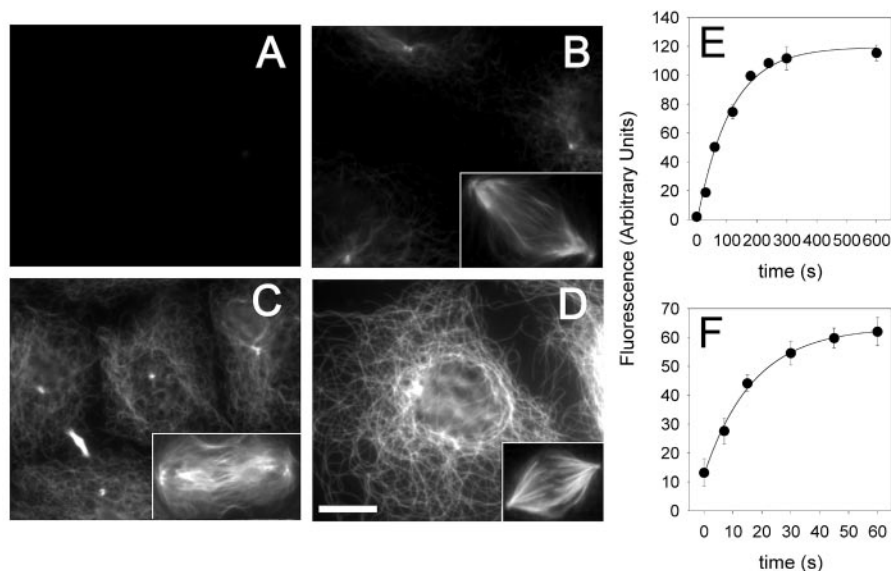
TABLE IV

Kinetic constants of fluorescent taxoid binding to (k_{+1}, k_{+2}) and dissociation from (k_{-1}, k_{-2}) MAP-containing microtubules in AB

		32 °C	35 °C	37 °C	39 °C	42 °C
Flutax-1	k_{+1} ($\times 10^5$ M^{-1} s^{-1})	1.54 ± 0.08	1.98 ± 0.07	2.28 ± 0.10	2.62 ± 0.03	3.18 ± 0.08
	k_{-1} (s^{-1})	0.19 ± 0.29	0.36 ± 0.31	0.61 ± 0.19	0.90 ± 0.10	1.06 ± 0.20
	k_{+2} (s^{-1})	1.29 ± 0.17	1.99 ± 0.56	2.37 ± 0.15	2.60 ± 0.15	3.16 ± 0.10
Flutax-2	k_{+1} ($\times 10^5$ M^{-1} s^{-1})	2.69 ± 0.23	2.73 ± 0.09	3.29 ± 0.19	3.97 ± 0.81	5.64 ± 0.46
	k_{-1} (s^{-1})	0.13 ± 0.29	0.30 ± 0.07	0.44 ± 0.31	0.56 ± 0.21	0.83 ± 0.72
	k_{+2} (s^{-1})	1.74 ± 0.14	2.10 ± 0.24	2.47 ± 0.70	2.65 ± 0.62	3.06 ± 0.51

		20 °C ($\times 10^{-2}$ s^{-1})	25 °C ($\times 10^{-2}$ s^{-1})	30 °C ($\times 10^{-2}$ s^{-1})	35 °C ($\times 10^{-2}$ s^{-1})	37 °C ($\times 10^{-2}$ s^{-1})	40 °C ($\times 10^{-2}$ s^{-1})	42 °C ($\times 10^{-2}$ s^{-1})
Flutax-1	k_{-2}	0.36 ± 0.04	0.72 ± 0.07	1.45 ± 0.02	2.77 ± 0.20	4.21 ± 0.10	5.67 ± 0.20	6.23 ± 0.20
Flutax-2	k_{-2}	0.49 ± 0.04	1.04 ± 0.05	1.40 ± 0.03	2.10 ± 0.15	2.34 ± 0.10	3.96 ± 0.30	4.07 ± 0.20

TABLE V

Thermodynamic parameters of binding of Flutax-1 and Flutax-2 to its site in microtubules assembled from microtubule protein in AB

	Flutax-1	Flutax-2		Flutax-1	Flutax-2
Ea_1 kJ mol^{-1}	58 ± 2	61 ± 12	Ea_2 kJ mol^{-1}	69 ± 9	45 ± 3
Ea_{-1} kJ mol^{-1}	142 ± 19	145 ± 16	Ea_{-2} kJ mol^{-1}	103 ± 3	76 ± 45
ΔH_1 kJ mol^{-1}	−84 ± 19	−84 ± 20	ΔH_2 kJ mol^{-1}	−34 ± 12	−31 ± 6
ΔS_1 J mol^{-1} K^{-1}	−151 ± 58	−154 ± 19	ΔS_2 J mol^{-1} K^{-1}	−55 ± 25	−52 ± 29
ΔH_{ovr} kJ mol^{-1}	−119 ± 22	−115 ± 21			
ΔS_{ovr} J mol^{-1} K^{-1}	−206 ± 63	−206 ± 96			

FIG. 6. **Representative images of the time course of 200 nM Flutax-2 binding (*A–D*) to cytoskeletons of PtK2 interphase cells.** *A*, 0-s incubation in Flutax-2; *B*, 30-s incubation; *C*, 1-min incubation; *D*, 10-min incubation. The *bar* represents 10 μm. *E*, time course of the averaged fluorescence intensity of cytoskeletons of interphase PtK2 cells upon incubation with 200 nM Flutax-2. *F*, time course of averaged fluorescence intensity of cytoskeletons of interphase PtK2 cells upon incubation with 1 μM Flutax-2. The nonspecific fluorescence measured with 50 μM docetaxel (19 arbitrary units on average) has been subtracted from the data. The *solid lines* are the best fitting to a single exponential curve.

mechanism of Taxol binding to microtubules is unknown, it had to be assumed that it consists of a single-step reaction in order to calculate the thermodynamic parameters (Table II), which have to be considered with this caution. Nevertheless, the linearity of the Arrhenius plots (Fig. 2*A*) and the compatibility of the kinetic data with the equilibrium measurements suggest that a single reaction (or a first step of a two-step reaction) is in fact being observed. The apparent reaction profile of Taxol binding is similar to the first step of Flutax-1 and Flutax-2 binding (not shown; see Ref. 35). This strongly supports the idea that this step mainly corresponds to the binding of the Taxol moiety of the fluorescent derivatives. It has to be pointed out that the activation energy of the binding of Taxol is lower, indicating a easier entrance of the smaller ligand to its site. The free energy of the binding of Taxol at 37 °C is around −45 kJ mol^{-1}, compatible with a predicted value $\Delta G \leq −48$ kJ mol^{-1} (53). The binding reaction of Taxol is endothermic, which explains why Taxol induces microtubule assembly at low temperatures, because the binding compensates for the decrease in the free energy of assembly (the extrapolated binding affinity of Taxol at 4 °C is 7.6×10^8 M^{-1}, so it may contribute to the

overall assembly-binding linked process with −47 kJ mol^{-1}).

In a diffusion-controlled reaction, the binding rate of a small ligand to an accessible site in a relatively immobilized molecule depends on the diffusion coefficient of the ligand and also on the efficiency of the collisions. The diffusion constant of Taxol is 20% larger than those of Flutax-1 and Flutax-2. Because Flutax-1, Flutax-2, and Taxol compete for the same site and the surface areas of Flutax-1 and Flutax-2 are 40% larger than that of Taxol, assuming that the effective surface for binding is the same, the efficiency of collision is expected to be 1.4 times larger for Taxol. The combination of the larger diffusion constant with better collision efficiency renders an expected kinetic rate of association 1.7 times larger for Taxol than for Flutax-1 and Flutax-2 (if the reaction is diffusion-colliding controlled and the observed step is the binding of the Taxol moiety of the molecule). The observed ratio is larger, which implies lower efficiency than expected for Flutax. There are two possible reasons for this, the first one is that Taxol and Flutax might have to pass through a pore of a restrictive size. Because their sizes are different, the flux of Taxol through the pores would be larger. However, this does not explain the dependence

FIG. 7. **Representative images of time course of Flutax-2 dissociation (*A–E*) from PtK2 cytoskeletons in the presence of 13.3 μM docetaxel.** *A*, 0-s incubation; *B*, 30-s incubation; *C*, 1-min incubation; *D*, 4-min incubation. The *bar* represents 10 μm. *E*, time course of averaged fluorescence intensity of cytoskeletons of interphase PtK2 cells labeled with Flutax-2 upon incubation in 13.3 μM docetaxel.
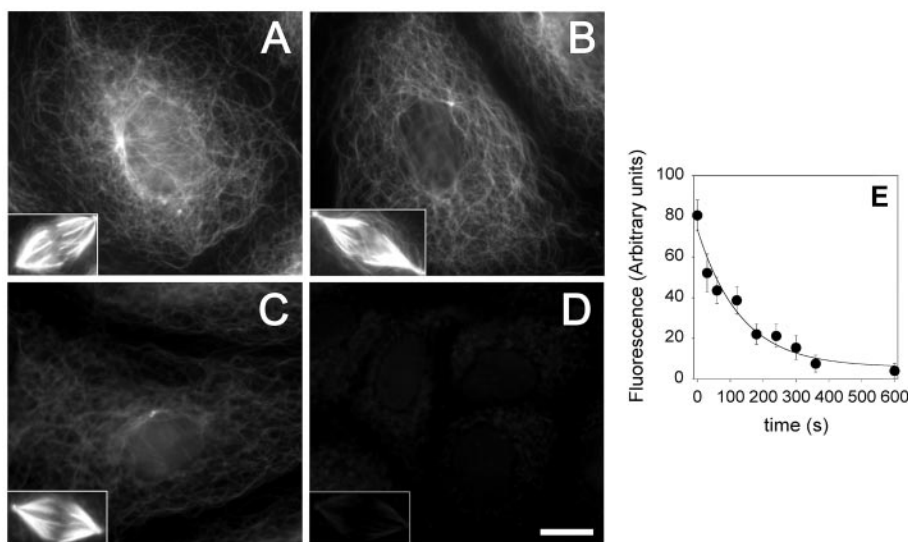
on temperature observed (k_{+1} (Taxol)/k_{+1} (Flutax-2): 25 °C 11.5, 30 °C 7.3, 35 °C 5.2, 37 °C 2.6, 40 °C 2.7), unless the pore size is temperature-dependent. In addition, diffusional flux through a pore of a size similar to those of the ligands in the microtubule wall (31) will not allow the binding reaction at the observed kinetic rate (35). A second, more feasible explanation is that the fluorescein moiety is hindering the binding of the Taxol moiety, perhaps by collapsing over it, as suggested by the small difference in the Stokes radii of Flutax and Taxol (8 and 7 Å, respectively). The activation energy of the first step of the binding of Flutax is larger than that of Taxol. This increase may indicate the existence of active and inactive conformations of Flutax. Such conformational equilibrium, if fast enough, will not alter the observed kinetic mechanism but only reduce the observed rate constant. If this equilibrium is influenced by the temperature, this will also explain the differences in the measured activation energy of the observed reaction.

The Location and Access of the Taxol-binding Site of Microtubules; Contradiction between Structural Models and Kinetic Results—Early low resolution microtubule models (45, 54) placed the Taxol-binding site at the interprotofilament space of microtubules. A compatible location was observed in a projection difference map of zinc-induced tubulin sheets at 6.5 Å resolution (55). Such location of the binding site would be compatible with the presently established fact that taxoids are able to access their binding site very rapidly. But since the three-dimensional high resolution model of microtubules appeared (31), one apparent contradiction showed up. The binding site of Taxol, one of the most effective drugs in favoring microtubule assembly, was mapped into the lumen of the tube, hidden from the outer solvent. It was suggested that rapid luminal access could occur via fenestrations in the microtubule wall (31). The three-dimensional structure of tubulin dimer, the location of the Taxol-binding site in the tertiary structure of β-tubulin, and the alignment of dimers to form protofilaments (23, 25, 27, 56–58) are all together hardly questionable. However, the association rate constants of the fluorescent derivatives of Taxol, Flutax-1, and Flutax-2 to the Taxol-binding site of microtubules, in the order of 10^6 M^{-1} s^{-1}, have been shown to be quantitatively incompatible with these ligands entering through the open microtubule ends or through fenestrations in the microtubule wall of 25 Å diameter (33–35). A simple way to place the Taxol-binding site of β-tubulin near the microtubule surface, *i.e.* a large rotation of the protofilament that would be needed in order to expose Taxol to the outer solvent (see Fig. 10 in Ref. 35), has been shown to be incompatible with several fits

of the same tubulin structure into microtubules performed with different microtubule density maps and fitting strategies (30, 31, 59). The current microtubule models indirectly account for the well known fact that Taxol has negligible affinity for isolated $\alpha\beta$-tubulin dimers but high affinity for microtubules or zinc-induced sheets (51, 60–62), through the contacts made by the M-loop (31, 63–64).

The results of the present work prove, we believe beyond any reasonable doubt, that Taxol binds to microtubules at a site which is directly accessible from the bulk of the solution. (i) The association rate of Taxol to microtubules is slightly faster than those of the rapidly binding fluorescent derivatives. (ii) The association of the fluorescent taxoids has been shown to be diffusion-controlled and significantly slowed down by MAPs, known to bind at the microtubule surface and to reduce the microtubule dynamics. (iii) The study has been extended to native microtubules prepared from cultured cells, which bind fluorescent taxoid at a similarly high rate, indicating an equally accessible Taxol-binding site, although it should be noted that microtubule cytoskeletons from cultured cells and microtubular protein have typically different tubulin isotypes, post-translational modifications, and MAPS (51). In addition, although the electron micrographs of microtubules assembled *in vitro* from pure tubulin typically show many areas in which the tube is open, which in principle provides a better access of the ligand through these areas, the labeling of the Ptk2 cell microtubules by the fluorescent taxoid is spatially homogeneous, indicating that all parts of the microtubules are equally accessible.

Very recently it has been argued that the fenestrations in the microtubule wall allow the passage of Taxol for binding at the microtubule lumen (65). However, the relevant issue here is not whether the fenestrations may eventually allow the ligand to squeeze in, but whether the ligand diffusion through them can be rapid enough to account for the fast binding observed. We previously discarded ligand passage through the holes (35) because at that time the size of the observed fenestrations in microtubule walls was roughly 10 Å (66), smaller than the 15 Å shortest dimensions of Flutax and Taxol. Let us now reexamine this possibility in view of the refined structure of tubulin dimers (23), the 14-Å microtubule map (30), the 8-Å microtubule map (65), and an independent model of microtubule structure (59). Fig. 8 shows a comparison of the dimensions of the taxoids used in this work with the fenestrations in a model microtubule wall. The size of the pores is comparable with the
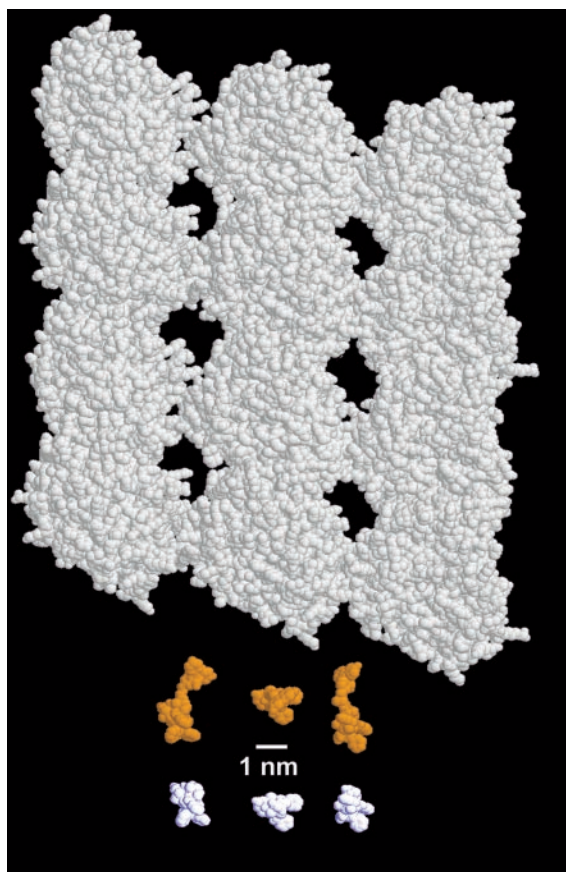
FIG. 8. **Pores in the microtubule surface.** van der Waals representation of the outer surface of a fragment of a high resolution microtubule model (55). For a comparison of the sizes of Flutax, Taxol, and the pores, the ligands are represented at the same scale in three different projections; *orange beads* indicate Flutax, and *white beads* indicate Taxol.

shortest dimension of the ligands; therefore, these pores should strongly restrict ligand diffusion through them.

To make an estimation of the order of magnitude of the maximum kinetic rate of binding of Taxol to a luminal microtubule site, it is convenient to divide the process into three steps with different factors whose product gives the rate constant: (*a*) the diffusion-limited ligand-microtubule encounter, (*b*) the efficiency of passage through the pores, and (*c*) the efficiency of productive collisions with the luminal binding site.

(*a*) For diffusion-limited ligand collision with microtubules, a maximum estimation for the rate constant value for a bimolecular reaction between Flutax and tubulin assembled in microtubules is 6.4×10^7 M^{-1} s^{-1} under our experimental conditions (see Equation 3 in Ref. 35). Note that due to the association of the tubulin subunits into an aggregate, this is smaller than the $\sim 4 \times 10^9$ M^{-1} s^{-1} value that can be estimated as a hypothetical diffusion limit for the binding of Taxol to unassembled tubulin (67). The frequency of collision of a small molecule with a large aggregate depends on the diffusion coefficient of the small molecule and the radius of collision, which can be approximated by the effective radius of the aggregate. The decrease of the rate of collision with the number of subunits in several polymers can be calculated by means of classical approaches (67, 68). In order to obtain the collision rate of the ligand with the subunit in the aggregate, the collision rate with the aggregate has to be divided by the number of subunits. The effective radius of the aggregate divided by the number of subunits is not constant but markedly decreases with the size of the aggregate, at a rate that depends on its geometry. Therefore,

polymerization results in a decrease of the diffusion limit of the bimolecular rate constant of ligand binding per subunit (see Fig. 10 and "Appendix").

(*b*) Regarding the efficiency of ligand passing through microtubule pores, in order to match the experimental association rate constant of 1.4×10^6 M^{-1} s^{-1} (35) with the 6.4×10^7 $M^{-1}s^{-1}$ diffusion limit, 2.2% of effective collisions between Flutax and microtubules is required. Similarly, 5.1% of effective collisions of Taxol with microtubules is needed to match the measured rate constant of 3.6×10^6 M^{-1} s^{-1} (see "Results"). A collision efficiency of 2–5% would be reasonable for taxoid binding at the microtubule surface, accounting for the percentage of surface area of microtubules forming the binding interface (35). The minimum pore sizes that may provide efficiencies in this range for ligand passing through them can be estimated from simple geometrical calculations of effective surface and angle of passage (35). For example, a 32 (diameter) $\times$ 30-Å (deep) cylindrical pore (which is of a size nearly comparable with a tubulin monomer) would allow 2.2% of successful collisions of a Flutax-equivalent 16-Å diameter sphere, resulting in ligand diffusion into the microtubule lumen. A 30-Å deep truncated and cone-shaped pore with 20-Å inner diameter and 32-Å outer diameter would lead to 1.9% of successful collisions. A more realistic (65) pore of truncated cone shape, say 30 Å (deep) $\times$ 17-Å inner diameter and 20-Å outer diameter, would have an efficiency of only 0.08% successful collisions, yielding a diffusion limit to the association rate constant of 5×10^4 M^{-1} s^{-1}, which is 2 orders of magnitude smaller than the observed value.

(*c*) Due to the efficiency of collision with the binding site, accounting in each of the above cases for the orientation and kinetic energy factors of the collision of the internalized ligand with the luminal binding site will further reduce the effective rate constant by order(s) of magnitude (69, 70). Therefore, in order to allow the ligand flux required to account for the observed binding reaction, the openings in the microtubule wall would have to be totally non-restrictive, *i.e.* much larger than the ligands. Otherwise the low efficiency of ligand passing through the pores reduces the kinetic rate of binding by several orders of magnitude below the experimentally observed value. Such non-restrictive openings are certainly larger than the pores in the model of Chacón and Wriggers (17 Å (59); Fig. 8) or in the electron microscopy maps of Meurer-Grob *et al.* (30) (about 15 by 25 Å) and Li *et al.* (65) ($\sim$17 Å). This analysis shows that it is not possible for Taxol to passively diffuse through the presently known microtubule fenestrations rapidly enough to bind at a luminal site at the observed rate.

In summary, the puzzle remains of how taxoids bind so rapidly to an apparently inaccessible model binding site at the microtubule lumen. We offer and analyze three hypotheses to potentially reconcile the fast kinetics of Taxol binding with a Taxol-binding site at the microtubule lumen. (i) The Taxol-binding site is exposed in unliganded microtubules, but it is buried following Taxol binding. (ii) The microtubule inside dynamically opens to the solvent so that the lumen is not a separate solution compartment. (iii) There is an initial Taxol-binding site (or channeling) at the microtubule surface that facilitates its transport into the lumen.

Does the Taxol-binding Site Become Inaccessible After Binding?—It might be conceivable that the Taxol-binding site is exposed in unliganded microtubules but buried in the Taxol bound ones. When Taxol binds rapidly to microtubules, they are known to undergo a slow conformational change entailing the loss of one protofilament on average (33), which may as well internalize the binding site. This type of binding mechanism is formally equivalent to Equation 1 (Introduction). Although this

hypothesis may appear as an easy explanation, there are several lines of experimental evidence against it. First, the wall structure of Taxol-induced microtubules is similar to that of drug-free microtubules at 30-Å resolution (54), except for the change in the number of protofilaments. Second, the binding of docetaxel, a side chain analog of Taxol, does not induce this diameter change in microtubules, indicating that the Taxol-induced change is restricted to the rearrangement of the subunits to compensate for the loss of one protofilament (33, 45). Third, both 14-Å resolution electron cryomicroscopy maps of microtubules stabilized by GMPCPP and by docetaxel have similar fenestrations (30).

Does Taxol Bind to an Internal Site via Large Dynamic Openings in the Microtubule Wall?—The hypothesis that Taxol accedes to its binding site via openings or defects in the microtubule wall was considered in our early publication (Fig. 7*D* in Ref. 33) and by Nogales *et al.* (31) to justify the fast binding. Two causes that might in principle contribute to the formation of such large pores, in the size range of tubulin monomers, are as follows.

(*a*) In the refined structure of tubulin at 3.5-Å resolution (23), several features involved in protofilament interactions in the microtubule (the M-loop and the loop between H1 and S2) have been retraced, and a Zn^{2+} ion has been found interacting with the M-loop of the α-subunit of tubulin. This ion should distort the natural lateral interaction between protofilaments, so that tubulin assembles into zinc sheets instead of microtubules. Because the microtubule models have been constructed using the tubulin dimer structure obtained from these zinc-induced sheets, the real lateral interactions between the tubulin dimers in microtubules, which have no zinc bound, should be different, and fenestrations larger than in the models might exist. The electron microscopy structure of Taxol-stabilized microtubules at 8 Å resolution (65) indicates a large reorganization of the Taxol-binding site with respect to the electron crystallographic structure of tubulin zinc sheets, including helix H6 and the M loop. There is a density in the averaged α- and β-tubulin monomer that corresponds to part of the regions occupied by Taxol in the β-tubulin structure and the B9-B10 peptide loop in α-tubulin, which is apparently backed by holes of comparable size (see Figs. 6*B* and 9*A* in Ref. 65). However, the fenestration size is still restrictive, not allowing ligand passage at the required kinetic rate (see above).

(*b*) The interprotofilament contacts in the microtubules may be so weak that large openings might be continuously appearing and closing in the microtubule wall. Lattice defects such as longitudinal shifts between protofilaments and changes in the number of protofilaments within single microtubules have been observed by cryo-electron microscopy, suggesting the weakness of the interprotofilament contacts (71–73). If such openings were not periodical, they would not be easily observed in electron micrographs of microtubules without Taxol bound.
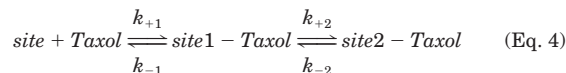
This explanation would be supported by the observation that microtubules are able to rapidly change the number of their protofilaments in response to taxoid binding (33). Even if cross-linking of microtubules would stabilize these interprotofilament contacts, microtubules would probably be frozen by fixation in a given situation, which would not affect the kinetics of the reaction, because the openings would be frozen. On the other hand, interprotofilament contacts would be expected to be stabilized by the presence of MAPs, which slow down the binding reaction and are known to block the ligand-induced changes in the number of protofilaments (54). Because these contacts would be stabilized as well by the taxoids, the taxoid off-rate could be similar in both types of microtubules, as observed.

In this way it might be possible that large holes open and close in the microtubule wall, resulting in a non-restrictive pore, so that the lumen ceases to be a separate chemical compartment. From a kinetic point of view, this is equivalent to adding a monomolecular pre-equilibrium step before the bimolecular binding event in the scheme of Equation 1 (Introduction), consisting of the conversion of inactive (closed) into active (open) binding sites. For this equilibrium to have passed undetected in the kinetic analysis of taxoid binding, it would have to be either extremely slow or have a rate constant k_0 more than 10-fold larger than the next step, that is $k_0 \geq 10 \cdot k_1 \cdot [ligand]$, which from typical values (35) is in the order of $k_0 \geq 100 \text{ s}^{-1}$. The hypothesis is not supported by the fact that the presence of a larger percentage of open areas in cross-linked frozen and melted microtubules results in the same kinetic rate of binding as in non-frozen ones. In addition, differences in the tubulin isoforms and post-translational modifications, between tubulin from brain and from cultured cells (51), which are known to affect the stability and dynamics of the microtubules (74, 75), are not reflected in the kinetics of binding of Flutax-2. This hypothesis of dynamic openings of non-restrictive size for ligands may be tested measuring the accessibility of the Taxol-binding site to macromolecular probes, whose size would hinder entering the microtubule lumen even through such holes.

These openings would not correspond to the so-called "seam" of the microtubules, because microtubules with the 3-start helix, B-lattice, and 13 protofilaments, which are the majority in the conditions of the study, do not have a seam (52, 73) and would be expected to bind taxoids at a slower rate. Control experiments in which the cross-linked microtubules stained with Flutax-2 were observed both by fluorescence and phase contrast showed that all microtubules were immediately stained after Flutax-2 addition. Even more, because transitions in the number of protofilaments within a single microtubule are common (73), it would be expected that dark and bright areas would be observed, which is not the case (see Fig. 1, Ref. 44).

Does Taxol Bind to an External Microtubule Site Before Binding at the Lumen?—The calculations above and even a simple visual inspection of the molecular models shown in Fig. 8 suggest the following: (*a*) for the ligand molecules randomly impinging onto the microtubule wall due to thermal motion, the statistical mechanical efficiency of passing through the model pores must be very low; (*b*) the ligand molecules hitting the holes should experience repulsive or attractive local interactions. It may not be totally unrealistic to hypothesize that some of them may fit and reside for some time into the pores. This last hypothesis is the same as binding to an initial external site in microtubules, which may facilitate transport to the luminal site. In this hypothetical mechanism, binding to the external and luminal sites should be mutually exclusive, because only 1.0 Taxol or Flutax molecules bind per tubulin dimer (12, 35), and Taxol or docetaxel prevents the binding of Flutax (35, 44). This could be accomplished if both sites shared an element that switches between the two alternative modes of binding.

This mechanism is identical to the one presented in Equation 1 (Introduction) at the resolution of the kinetic methods employed, substituting the second step by the ligand exchange from the first into the second site (Equation 4).

$$site + Taxol \underset{k_{-1}}{\overset{k_{+1}}{\rightleftharpoons}} site1 - Taxol \underset{k_{-2}}{\overset{k_{+2}}{\rightleftharpoons}} site2 - Taxol \quad \text{(Eq. 4)}$$

Flutax might be able to bind at the external site and then be internalized, in which case the second step of Flutax binding
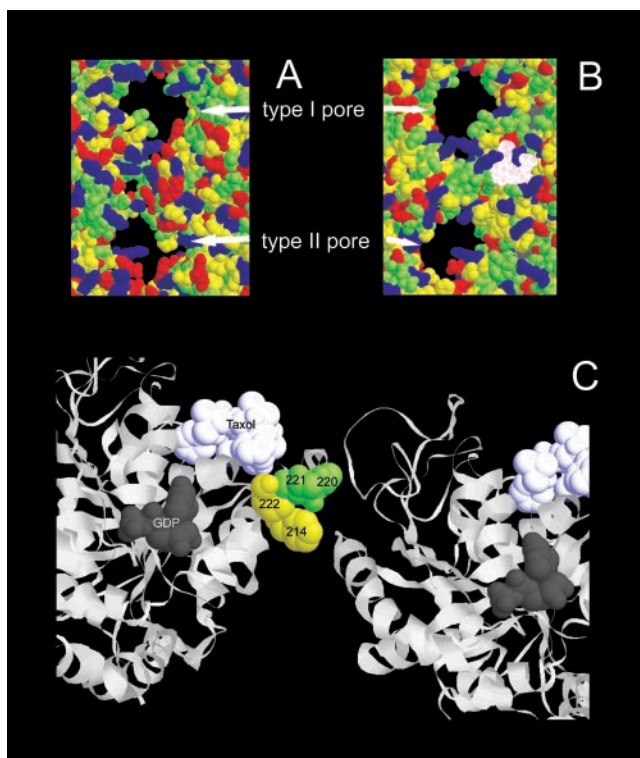
FIG. 9. Insight of the outer and inner surface (*A* and *B*) of a high resolution microtubule model (55) showing two different types of pores, I and II (see text). *Green beads*, polar residues; *yellow beads*, hydrophobic residues; *red beads*, acid residues; *blue beads*, basic residues; *white beads*, Taxol bound at its site; *gray beads*, nucleotide. *C*, detail of a type I pore viewed from above. Ribbon representation of two neighbor β-tubulin subunits as seen from the plus end of the microtubule; Taxol, GDP, and the four residues forming a putative taxoid-binding site are shown in van der Waals representation.

FIG. 10. **Dependence of the collision rate between a small molecule and a protein polymer on the size of the polymer.** *Solid line,* microtubules; *dashed line,* linear aggregate; *dotted line*, hollow spherical aggregate.

would correspond to ligand internalization, or it may be sterically or otherwise hindered from internalization, in which case the second step would correspond to the binding of the fluorescein moiety at the microtubule surface. Both cases are kinetically equivalent for our experimental set up, in which the second step is a structural rearrangement that restricts the conformational freedom of the fluorescent moiety of Flutax resulting in the observed increase of the fluorescence anisotropy of the probe (35).

A conformational change after Taxol binding will probably alter the interprotofilament contacts resulting in alterations of the number of protofilaments as observed (33, 35, 45, 54); the large fluorescent moiety of Flutax probably interacts as well with residues close to the interprotofilament space resulting into even larger modifications in the number of protofilaments (35). The Taxol-binding site ligands sarcodictin, epothilone B, and eleutherobin have related effects in the number of protofilaments of microtubules (30) suggesting a similar mechanism of binding.

Let us analyze which pores and which elements of the microtubule wall may take part in the Taxol binding process. As shown in Fig. 9, the microtubule outer surface near the pores (Fig. 9*A*) appears generally to be less hydrophobic than the luminal surface (Fig. 9*B*). Microtubules have mainly a type B lattice (76–79) with two different types of pores (Fig. 9, *A* and *B*). In type I pore the β-subunit is at the lower part of the pore (with the microtubule oriented with its plus end upwards), and the luminal Taxol-binding site is closer to the pore than in type II pore, where the α-subunit is at the lower part of the fenestration. Looking from the outside (Fig. 9*A*), a main chemical difference between both types of pores is located at the loop
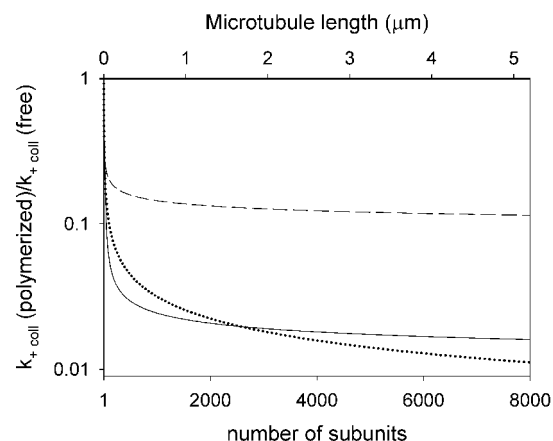
between helix H6 and H7, consisting of residues 214–223, which is at the left lower part of the pore. The Leu-217 and Leu-219 β-tubulin residues make hydrophobic contact with the 2-benzoyl ring of Taxol in the zinc sheets (23). This loop has also been proposed to take part in the lateral contacts between the protofilaments (30, 31). The loop is more charged in the α-subunit (5 charged residues of 10) than in the β-subunit (2 charged residues of 10). It forms a prominence into the pore with an acid part and a basic part in the type II pore, whereas in the type I pore it has a hydrophobic part (Phe-214, Leu-215, Leu-217, Leu-219, and Pro-222) (which corresponds with the acid part in the α-subunit) and a polar part (Thr-220 and Thr-221) (which corresponds to the basic part in the α-subunit) (Fig. 9, *A* and *B*). Mutations that introduce charged residues at this loop of the β-subunit (L215H, L217R, L219R) conferred Taxol resistance, whereas a conservative mutation L217F resulted in a Taxol-dependent cell line (57, 58). It is conceivable that the H6-H7 loop of β-tubulin could adopt different conformations in Taxol-free microtubules, presenting a binding surface that may be part of the initial Taxol-binding site. Let us now examine a possible way in which a Taxol molecule may bind to the H6-H7 loop from the outside of the microtubule. Three parts can be distinguished in the so-called hydrophobically collapsed conformation of taxoids, which is suggested by NMR analysis to be the dominant contribution to the conformational average in aqueous solution and is distinct from the proposed microtubule-bound conformations (80) (see Fig. 5 in Ref. 80; Fig. 1*A* in Ref. 81): (i) the hydrophobic cluster formed by the 2-*O*-benzoyl, 3′-phenyl, and 4-*O*-acetyl groups; (ii) a more hydrophilic zone that includes the polar groups of the side chain at C-13; and (iii) the part that contains the non-essential substituents at positions C-7 and C-10. A more detailed insight into the type I pore (Fig. 9*C*, looking from above) shows that the side chains of residues Phe-214, Thr-220, Thr-221, and Pro-222 form an almost equilateral triangle of 7 Å side with hydrophobic vertexes in Phe-214 and Pro-222 and polar vertex in the threonines. This distance of 7 Å is very similar to the sides of the triangles formed by the 2-OH group of Taxol and any two of the three phenyl groups of the hydrophobic cluster. It is tempting to speculate that the hydrophobic cluster of Taxol may initially bind to the hydrophobic residues of the H6-H7 loop, with the threonines at the right distance to interact with the 1′ and 2′ oxygens and/or the 3′ carbamate group of the C-13 Taxol side chain. Note that a free 2′-OH group is essential for the recognition of taxoids by microtubules (81).

Loop H6-H7 is flanked by Gly-225, which might be an excel-

lent hinge point for a conformational transition. The molecular flexibility of tubulin in the presence and absence of Taxol has been studied using normal mode analysis (82). This conformational analysis has pointed at threonines 220 and 221 among the most flexible residues of the β-subunit, showing large differences in flexibility against their counterparts in the α-subunit. In the recent structure of microtubules at 8 Å, the most prominent difference from the zinc sheets is the loss of density and contacts of helix H6 and the H6-H7 loop, suggesting that this region may be flexible in the microtubule (65). In the hypothetical mechanism of facilitated transport of Taxol, the H6-H7 loop would be a lid that swings the ligand from the pore into the luminal binding site.

It should be noted that in this hypothesis the external Taxol-binding site is directly conformed by the microtubule pores, which are not present in tubulin dimers or in linear oligomers. This type of mechanism would have profound implications for microtubule structure and anti-cancer drug design, because the different types of Taxol-mimetic compounds (13–16) and even different taxanes could have preferential affinity for the first or second Taxol-binding sites. The hypothesis may be scrutinized by means of advanced stopped-flow kinetic methods. For example, because the second step of Flutax-1 and Flutax-2 binding is much slower than the first step, it could be possible to trap the possible intermediate species in the reaction, by using a probe that binds quickly to the fluorescent moiety of the ligand, such as an antibody that quenches the fluorescence, and will allow the comparison between the exposure of the fluorescein group in the intermediate state and that of the final bound state. If this hypothesis is correct the kinetics of binding of the antibody to the intermediate state would be significantly different from that of binding to the end state.

This hypothesis and the preceding one, speculative as they are, constitute the two explanations we have thought may reconcile the observed fast kinetics of Taxol binding with the current microtubule models. Unequivocally mapping Taxol, fluorescent taxoids and possible reaction intermediates, in the structure of microtubules (instead of the zinc sheets) would illuminate this problem.

APPENDIX

For the decrease of ligand collision rate by protein polymerization, the collision rate of a small ligand with different protein assemblies can be calculated as described (67), neglecting the diffusion coefficient of the large molecule or polymer and introducing modifications that account for the polymer geometry (68).

For the case of a hollow spherical polymer, the colliding rate of the ligand per assembled subunit ($k_{+\text{coll}}$ (M^{-1} s^{-1})) can be approximated by Equation A1,

$$k_{+\text{coll}} = \frac{4 \cdot \pi \cdot R \cdot D \cdot 1000 \cdot Na}{n} \qquad \text{(Eq. A1)}$$

where R is the radius of the sphere in meters; D is the diffusion constant of the ligand (in m^2 s^{-1}); Na is Avogadro's number; and n is the number of subunits. For a hollow sphere the surface is linearly related to the number of subunits, $S = a \cdot n$, where a is the exposed collision surface of each subunit. Be-

cause the radius of a sphere is $r = (S/4 \cdot \pi)^{1/2}$, by substituting into Equation A1, it can be calculated that the dependence of $k_{+\text{coll}}$ with the number of subunits is as shown in Equation A2,

$$k_{+\text{coll}} = \frac{\sqrt{4 \cdot \pi \cdot a \cdot D \cdot 1000 \cdot Na}}{\sqrt{n}} \qquad \text{(Eq. A2)}$$

and Equation A3,

$$\frac{k_{+\text{coll}}(\text{assembled})}{k_{+\text{coll}}(\text{free})} = \frac{1}{\sqrt{n}} \qquad \text{(Eq. A3)}$$

as it is indicated by the *dotted line* in Fig. 10.

A linear oligomer can be approximated by a long ellipsoid (68), where the colliding rate per subunit becomes (Equation A4),

$$k_{+\text{coll}} = \frac{2 \cdot \pi \cdot L \cdot D \cdot 1000 \cdot Na}{Ln\left(\frac{L}{r}\right) \cdot n} \qquad \text{(Eq. A4)}$$

where L is the length of the ellipsoid, and r is its small semi-axis. Because r is constant and $L = b \cdot n$, where b is the longitudinal spacing between subunits, the dependence of $k_{+\text{coll}}$ with the number of subunits (Equation A5) is

$$k_{+\text{coll}} = \frac{2 \cdot \pi \cdot b \cdot D \cdot 1000 \cdot Na}{Ln(n) + Ln(b) - Ln(r)} \qquad \text{(Eq. A5)}$$

which decreases as shown by the *dashed line* in Fig. 10.

A helical polymer can be approximated as the linear oligomer except for the fact that $L = b \cdot n/t$, where t is the number of subunits per turn. The dependence of $k_{+\text{coll}}$ on the number of subunits is shown in Equation A6,

$$k_{+\text{coll}} = \frac{2 \cdot \pi \cdot b \cdot D \cdot 1000 \cdot Na}{t \cdot Ln(n) + Ln(b) - Ln(r) - Ln(t)} \qquad \text{(Eq. A6)}$$

This is illustrated for the case of a 12-protofilament microtubule ($b = 8$ nm, $r = 11.1$ nm, $t = 12$) by the *solid line* in Fig. 10, where the upper abscissa scale shows the microtubule length. It is concluded that for relatively compact polymers (spheres and microtubules), made of a few thousands subunits, the collision rate of the small ligand with an assembled subunit decreases by nearly 2 orders of magnitude with respect to the free subunit.

REFERENCES

1. Wani, M., C., Taylor, H. L., Wall, M. E., Coggon, P., and McPhail, A. T. (1971) *J. Am. Chem. Soc.* **93**, 2325–2327
2. Choy, H. (2001) *Crit. Rev. Oncol. Hematol.* **37**, 237–247
3. Schiff, P. B., Fant, J., and Horwitz, S. B. (1979) *Nature* **277**, 665–667
4. Correia, J. J., and Lobert, S. (2001) *Curr. Phar. Des.* **7**, 1213–1218
5. Borisy, G. G., and Taylor, E. W. (1967) *J. Cell Biol.* **34**, 525–533
6. Borisy, G. G., and Taylor, E. W. (1967) *J. Cell Biol.* **34**, 535–548
7. Wilson, L., and Friedkin, M. (1967) *Biochemistry* **6**, 3126–3135
8. Bensch, K. G., Marantz, R., Wisniewski, H., and Shelanski, M. (1969) *Science* **165**, 495–496
9. Jordan, M. A., Toso, R. J., Thrower, D., and Wilson, L. (1993) *Proc. Natl. Acad. Sci. U. S. A.* **90**, 9552–9556
10. Derry, W. B., Wilson, L., Khan, I. A., Ludueña, R. F., and Jordan, M. A. (1997) *Biochemistry* **36**, 3554–3562
11. Yvon, A. M., Wadsworth, P., and Jordan, M. A. (1999) *Mol. Biol. Cell* **10**, 947–959
12. Díaz, J. F., and Andreu, J. M. (1993) *Biochemistry* **32**, 2747–2755
13. Bollag, D. M., McQueney, P. A., Zhu, J., Hensens, O., Koupal, L., Liesch, J., Goetz, M., Lazarides, E., and Woods, C. M. (1995) *Cancer Res.* **55**, 2325–2333
14. Ter Haar, E., Kowalski, R. J., Hamel, E., Lin, C. M., Longley, R. E., Gunas-ekera, S. P., Rosenkranz, H. S., and Day, B. W. (1996) *Biochemistry* **35**, 243–250
15. Mooberry, S. L., Tien, G., Hernandez, A. H., Plubrukarn, A., and Davidson, B. S. (1999) *Cancer Res.* **59**, 653–660
16. Long, B. H., Carboni, J. M., Wasserman, A. J., Cornell, L. A., Casazza, A. M., Jensen, P. R., Lindel, T., Fenical, W., and Fairchild, C. R. (1998) *Cancer Res.* **58**, 1111–1115
17. Ojima, I., Chakravarty, S., Inoue, T., Lin, S., He, L., Horwitz, S. B., Kuduk, S. D., and Danishefsky, S. J. (1999) *Proc. Natl. Acad. Sci. U. S. A.* **96**, 4256–4261

18. He, L., Jagtap, P. G., Kingston, D. G., Shen, H. J., Orr, G. A., and Horwitz, S. B. (2000) *Biochemistry* **39,** 3972–3978
19. Giannakakou, P., Gussio, R., Nogales, E., Downing, K. H., Zaharevitz, D., Bollbuck, B., Poy, G., Sackett, D., Nicolaou, K. C., and Fojo, T. (2000) *Proc. Natl. Acad. Sci. U. S. A.* **97,** 2904–2909
20. He, L., Orr, G. A., and Horwitz, S. B. (2001) *Drug Discov. Today* **6,** 1153–1164
21. Pryor, D. E., O'Brate, A., Bilcer, G., Díaz, J. F., Wang, Y., Wang, Y., Kabaki, M, Jung, M. K., Andreu, J. M., Gosh, A. K., Giannakakou, P., and Hamel, E. (2002) *Biochemistry* **41,** 9109–9115
22. Snyder, J. P., Nettles, J. H., Cornett, B., Downing, K. H., and Nogales, E. (2001) *Proc. Natl. Acad. Sci. U. S. A.* **98,** 5312–5316
23. Löwe, J., Li, H., Downing, K. H., and Nogales, E. (2001) *J. Mol. Biol.* **313,** 1045–1057
24. Rao, S., Krauss, N. E., Heerding, J. M., Swindell, C. S., Ringel, I., Orr, G. A., and Horwitz, S. B. (1994) *J. Biol. Chem.* **269,** 3132–3134
25. Rao, S., Orr, G. A., Chaudhary, A. G., Kingston, D. G., and Horwitz, S. B. (1995) *J. Biol. Chem.* **270,** 20235–20238
26. Rao, S., He, L., Chatkravarty, S., Ojima, I., Orr, G. A., and Horwitz, S. B. (1999) *J. Biol. Chem.* **274,** 37990–37994
27. Nogales, E., Wolf, S. G., and Downing, K. (1998) *Nature* **391,** 199–203
28. Melki, R., and Carlier, M. F. (1993) *Biochemistry* **32,** 3405–3413
29. Sosa, H., Dias, D. P., Hoenger, A., Whittaker, M., Wilson-Kubalek, E., Sablin, E., Fletterick, R. J., Vale, R. D., and Milligan, R. A. (1997) *Cell* **90,** 217–224
30. Meurer-Grob, P., Kasparian, J., and Wade, R. H. (2001) *Biochemistry* **40,** 8000–8008
31. Nogales, E., Whittaker, M., Milligan, R. A., and Downing, K. H. (1999) *Cell* **96,** 79–88
32. Dye, R. B., Fink, S. P., and Williams, R. C. (1993) *J. Biol. Chem.* **268,** 6847–6850
33. Díaz, J. F., Valpuesta, J. M., Chacón, P., Diakun, G., and Andreu, J. M. (1998) *J. Biol. Chem.* **273,** 33803–33810
34. Evangelio, J. A., Abal, M., Barasoain, I., Souto, A. A., Acuña, A. U., Amat-Guerri, F., and Andreu, J. M. (1998) *Cell Motil. Cytoskeleton* **39,** 73–90
35. Díaz, J. F., Strobe, R., Engelborghs, Y., Souto, A. A., and Andreu, J. M. (2000) *J. Biol. Chem.* **275,** 26265–26276
36. Abal, M., Souto, A. A., Amat-Guerri, F., Acuña, A. U., Andreu, J. M., and Barasoain, I. (2001) *Cell Motil. Cytoskeleton* **49,** 1–15
37. De Pereda, J. M., Wallin, M., Billger, M., and Andreu, J. M. (1995) *Cell Motil. Cytoskeleton* **30,** 153–163
38. Sloboda, R. D., and Rosenbaum, J. L. (1982) *Methods Enzymol.* **85,** 409–416
39. Goedert, M., Spillantini, M. G., Potier, M. C., Ulrich, J., and Crowther, R. A. (1989) *EMBO J.* **8,** 393–399
40. Souto, A. A., Acuña, A. U., Andreu, J. M., Barasoain, I., Abal, M., and Amat-Guerri, F. (1995) *Angew. Chem. Int. Ed. Engl.* **34,** 2710–2712
41. Rickwood, D. (ed) (1989) *Centrifugation: A Practical Approach,* 2nd Ed., pp. 265–266, IRL Press at Oxford University Press, Oxford
42. Muramatsu, N., and Minton, A. P. (1988) *Anal. Biochem.* **168,** 345–351
43. Sheely, M. L. (1932) *Ind. Eng. Chem.* **24,** 1060–1064
44. Andreu, J. M., and Barasoain, I. (2001) *Biochemistry* **40,** 11975–11984
45. Andreu, J. M., Díaz, J. F., Gil, R., de Pereda, J. M., García de Lacoba, M., Peyrot, V., Briand, C., Towns-Andrews, E., and Bordas, J. (1994) *J. Biol. Chem.* **269,** 31785–31792
46. Walker, J. M. (1996) *The Protein Protocols Handbook,* pp. 101–107, Humana Press, Inc., Totowa, NJ
47. Bevington, P. R. (1969) *Data Reduction and Error Analysis for the Physical Sciences*, pp. 235–240, McGraw-Hill Book Co., New York
48. Barshop, B. A., Wrenn, R. F., and Frieden, C. (1983) *Anal. Biochem.* **130,** 134–145
49. De Ines, C., Leynadier, D., Barasoain, I., Peyrot, V., García, P., Briand, C., Rener, G. A., and Temple, C., Jr. (1994) *Cancer Res.* **54,** 75–84
50. Sullivan, K. F., and Cleveland, D. W. (1986) *Proc. Natl. Acad. Sci. U. S. A.* **83,** 4327–4331
51. Ludueña, R. F. (1998) *Int. Rev. Cytol.* **178,** 207–275
52. Strehlow, H., and Knoche, W. (1977) *Fundamentals of Chemical Relaxation*, pp. 47–67, Verlag Chemie, Weinheim, Germany
53. Díaz, J. F., Menéndez, M., and Andreu, J. M. (1993) *Biochemistry* **32,** 10067–10077
54. Andreu, J. M., Bordas, J., Díaz J. F., García de Ancos, J., Gil, R., Medrano, F. J., Nogales, E., Pantos, E., and Towns-Andrews, E. (1992) *J. Mol. Biol.* **226,** 169–184
55. Nogales, E., Wolf, S. G., Khan, I. A., Ludueña, R. F., and Downing, K. H. (1995) *Nature* **375,** 424–427
56. Giannakakou, P., Sackett, D. L., Kang, Y. K., Zhan, Z., Buters, J. T., Fojo, T., and Poruchynsky, M. S. (1997) *J. Biol. Chem.* **272,** 17118–17125
57. Gonzalez-Garay, M. L., Chang, L., Blade, K., Menick, D. R., and Cabral, F., (1999) *J. Biol. Chem.* **274,** 23875–23882
58. Monzó, M., Rosell, R., Sánchez, J. J., Lee, J. S., O'Brate, A., González-Larriba, J. L., Alberola, V., Lorenzo, J. C., Núñez, L., Ro, J. Y., and Martín, C. (1999) *J. Clin. Oncol.* **17,** 1786–1793
59. Chacón, P., and Wriggers, W. (2002) *J. Mol. Biol.* **317,** 375–384
60. Parness, J., and Horwitz, S. B. (1981) *J. Cell Biol.* **91,** 479–487
61. Manfredi, J. J., Parness, J., and Horwitz, S. B. (1982) *J. Cell Biol.* **92,** 688–696
62. Takoudju, M., Wright, M., Chenu, J., Guéritte-Voegelein, F., and Guénard, D. (1988) *FEBS Lett.* **234,** 177–180
63. Amos, L. A., and Lowe, J. (1999) *Chem. Biol.* **3,** 65–69
64. Snyder, J. P., Nettles, J. H., Cornett, B., Downing, K. H., and Nogales, E. (2001) *Proc. Natl. Acad. Sci. U. S. A.* **98,** 5312–5316
65. Li, H., DeRosier, D. J., Nicholson, W. V., Nogales, E., and Downing, K. H. (2002) *Structure* **10,** 1317–1328
66. Kikkawa, M., Okada, Y., and Hirokawa, N. (2000) *Cell* **100,** 241–252
67. Cantor, C. R., and Schimmel, P. R. (1980) *Biophysical Chemistry,* pp. 916–922, W. H. Freeman & Co., San Francisco, CA
68. Berg, H. C. (1983) *Random Walk in Biology*, pp. 17–36, Princeton University Press, Princeton, NJ
69. Northrup, S. H., and Erickson, H. P. (1992) *Proc. Natl. Acad. Sci. U. S. A.* **89,** 3338–3342
70. Janin, J. (1997) *Proteins Struct. Funct. Genet.* **28,** 153–161
71. Chrétien, D., Metoz, F., Verde, F., Karsenti, E., and Wade. R. H. (1992) *J. Cell Biol.* **117,** 1031–1040
72. Ray, S., Meyhöfer, E., Milligan, R., and Howard, J. (1993) *J. Cell Biol.* **121,** 1083–1093
73. Chrétien, D., and Fuller, S. D. (2000) *J. Mol. Biol.* **298,** 663–676
74. Lu, Q., and Ludueña, R. F. (1994) *J. Biol. Chem.* **269,** 2041–2047
75. Panda, D., Miller, H. P., Banerjee, A., Ludueña, R. F., and Wilson, L. (1994) *Proc. Natl. Acad. Sci. U. S. A.* **91,** 11358–11362
76. Kikkawa, M., Ishikawa, T., Nakata, T., Wakabayashi, T., and Hirokawa, N. (1994) *J. Cell Biol.* **127,** 1965–1971
77. Song, Y. H., and Mandelkow, E. (1995) *J. Cell Biol.* **128,** 81–94
78. Sosa, H., and Milligan, R. A. (1996) *J. Mol. Biol.* **260,** 743–755
79. Metoz, F., Arnal, I., and Wade, R. H. (1997) *J. Struct. Biol.* **118,** 159–168
80. Jiménez-Barbero, J., Amat-Guerri, F., and Snyder, J. P. (2002) *Curr. Med. Chem. Anti-Cancer Agents* **2,** 91–122
81. Jimenez-Barbero. J., Souto, A. A., Abal, M., Barasoain, I., Evangelio, J. A., Acuña, A. U., Andreu, J. M., and Amat-Guerri, F. (1998) *Bioorg. Med. Chem.* **6,** 1857–1863
82. Keskin, O., Durell, S. R., Bahar, I., Jernigan, R. L., and Covell, D. G. (2002) *Biophys. J.* **83,** 663–680